Constraints, metastability, and inherent structures in liquids

D. S. Corti, P. G. Debenedetti, and S. Sastry
Department of Chemical Engineering, Princeton University, Princeton, New Jersey 08544

F. H. Stillinger
Bell Laboratories, Lucent Technologies, Murray Hill, New Jersey 07974
and Princeton Materials Institute, Princeton University, Princeton, New Jersey 08544
(Received 23 December 1996)

Void-size distributions have been calculated for the shifted-force Lennard-Jones fluid over substantial temperature and density ranges, both for the liquid-state configurations themselves, as well as for their inherent structures (local potential energy minima). The latter distribution is far more structured than the former, displaying fcc-like short-range order, and a large-void tail due to system-spanning cavities. Either void distribution can serve as the basis for constraints that retain the liquid in metastable states of superheating or stretching by eliminating configurations that contain voids beyond an adjustable cutoff size. While acceptable cutoff sizes differ substantially in the two versions, ranges of choices have been identified yielding metastable equations of state that agree between the two approaches. Our results suggest that the structure-magnifying character of configuration mapping to inherent structures may be a useful theoretical and computational tool to identify the low-temperature mechanisms through which liquids and glasses lose their mechanical strength. [S1063-651X(97)03805-1]

PACS number(s): 61.20.Gy, 64.60.My, 64.70.Fx, 05.70.−a

I. INTRODUCTION

The formation, characterization, and utilization of metastable forms of matter present challenges and opportunities throughout science and technology. All phases are involved: solid, liquid, and vapor. The usefulness of a metastable substance in any given application normally depends on the ability to frustrate kinetic processes of phase change that cause reversion to thermal equilibrium. The phenomenological classical nucleation theory has enjoyed substantial success in predicting such rates of phase change under many circumstances of interest [1,2,3], but its connection to the rigorous molecular theory of matter remains incomplete. Indeed, many basic questions also remain about the nature of metastable states themselves [4].

The present paper reports results of a theoretical study designed to enrich fundamental understanding of liquids that are superheated (i.e., metastable with respect to nucleation and growth of the vapor phase). Real-world connections involve explosive boiling [5], cavitation in turbulent flow [5,6], bubble-chamber detectors for elementary particles [7], and the tensile behavior of sap rising in trees [8]. The initial stage of sonoluminescence experiments also involves cavitation, owing to ultrasonic excitation [9].

Section II below discusses the general theoretical strategy of imposition of constraints designed to prevent vapor nucleation in a superheated and/or stretched liquid and the influence of those constraints on measurable properties of the liquid. Primary interest in the present study focuses on spontaneously formed voids in the liquid medium, the largest of which must be prevented to frustrate nucleation. Section III shows how void-size constraints, both before and after configuration mapping to ''inherent structures'' [10,11], can be employed to effect the desired metastable extensions; comparisons of the two constraint versions are provided. Section IV presents results of an analysis of the statistical geometry of the shifted-force Lennard-Jones liquid, examined in both the equilibrium region of its phase-plane, as well as in the metastable extension regime into the region of equilibrium liquid-vapor coexistence. Void distributions have been obtained for all of these states, both for the liquid itself, as well as for the corresponding sets of inherent structures obtained by mapping particle configurations onto potential energy minima. The final section, Sec. V, summarizes our results, states our conclusions, and attempts to predict the most productive directions for further study.

II. CONSTRAINTS AND THEIR EFFECTS

Under conditions of strict thermal equilibrium, the properties of an N-body system can be represented by the canonical ensemble. It suffices for present purposes to suppose that the system comprises point particles (no internal degrees of freedom), and that the classical limit applies. Consequently, the canonical partition function Q in the following form provides the thermodynamic properties at temperature T and volume V [12]:

$$Q(N,V,T)=(N!\Lambda^{3N})^{-1}\int\cdots\int e^{-\beta\Phi_N}d\mathbf{r}_1\cdots d\mathbf{r}_N. \quad (1)$$

Here Λ is the mean thermal deBroglie wavelength; β is $1/kT$, k being Boltzmann's constant; and $\Phi_N(\mathbf{r}_1\cdots\mathbf{r}_N)$ is the interaction potential for the N particles located at $\mathbf{r}_1\cdots\mathbf{r}_N$. The integrals in Eq. (1) are restricted to the interior of volume V. The pressure equation of state emerges as a volume derivative,

$$P=\frac{1}{\beta}\left(\frac{\partial \ln Q}{\partial V}\right)_{N,T}; \tag{2}$$

in particular, this expression correctly captures the break in the pressure isotherms as the system crosses an equilibrium phase transition curve in the (V,T) plane.

Nucleating and growing a new phase at a first-order phase transition normally is kinetically difficult, provided the material under study is clean and mechanically undisturbed. Consequently, metastable extensions beyond the transition point, in temperature or density, are commonplace. The presence of a kinetic barrier to first-order phase change is tantamount to bimodality of the canonical probability distribution $\exp(-\beta\Phi_N)$, corresponding to virtually distinct and nonoverlapping contributions that reside in different regions of the N-body configuration space. The ''bottleneck'' region between them has a low probability of occupation, at least for modest extensions into metastability.

In order to achieve a reformulation of the canonical ensemble that accords with experimental observation of metastability, a mathematical device must be provided to close the bottleneck, thereby trapping the system's configuration in the appropriate one-phase region even as the location of an equilibrium phase change is passed. This constraint can always be attained in principle by imposing an additional potential on the N-body system, $W_N(\mathbf{r}_1\cdots\mathbf{r}_N)$, that vanishes in the desired one-phase region of the configuration space, but is positive and arbitrarily large in the region that displays at least some portion of the alternative and thermodynamically favored phase. The discontinuity locus for W_N in the $3N$-dimensional configuration space is a $(3N-1)$-dimensional hypersurface that dynamically acts as a reflecting boundary for the system point, returning it to the interior of the one-phase region.

The choice of specific form for the constraint potential W_N will be dictated by the metastable phase of interest. Supercooled liquids and the glasses they form must be free of all but the smallest recognizable crystallites, so W_N must become large whenever any substantial local set of particles displays crystalline order [11,13]. Supersaturated vapors require W_N to be large if any substantial cluster (droplet) of particles appears [2]. Superheated liquids, or liquids under tension, must be free of substantial voids or cavities, so W_N must become large if such patterns exist anywhere in the liquid medium [14,15]. This last case is the one examined in the following sections of this paper.

Having selected W_N for the application of interest, the modified canonical partition function Q^* has the obvious form

$$Q^*(N,V,T)=(N!\Lambda^{3N})^{-1}\int\cdots\int e^{-\beta(\Phi_N+W_N)}d\mathbf{r}_1\cdots d\mathbf{r}_N, \tag{3}$$

with the same integration limits as before. Because W_N has been chosen to be large and positive somewhere in the configuration space, but is non-negative everywhere, we have

$$0<Q^*<Q. \tag{4}$$

The metastable-state pressure corresponding to Q^* involves the direct analog of Eq. (2):

$$P^*=\frac{1}{\beta}\left(\frac{\partial \ln Q^*}{\partial V}\right)_{N,T}. \tag{5}$$

This constrained-ensemble pressure contains an ideal gas contribution, as well as contributions from the interparticle interactions (Φ_N) and from the constraint (W_N).

Most statistical-mechanical modeling of liquids (including the present study) assume that Φ_N consists only of additive pair terms, which for structureless particles requires

$$\Phi_N=\sum_{i>j}\sum_{j=1}^{N-1}\phi(r_{ij}), \tag{6}$$

where r_{ij} is the distance separating the centers of particles i and j. For some applications one might wish to assign a similar form to W_N. But as indicated above, attaining metastability generally requires W_N to realize a specific pattern-recognition capacity in much larger groups of particles than just pairs.

The volume derivative appearing in Eq. (5) can be handled by the same volume scaling tactic that has become standard practice for the unconstrained canonical ensemble [16]. Presuming that the volume V is cubical, the coordinate transformation

$$\mathbf{r}=V^{1/3}\mathbf{s} \tag{7}$$

causes the integrations in Q^*, Eq. (3), to span a unit cube in $\mathbf{s}$ space, while permitting the volume derivative to be carried out by the chain rule. The result of these operations may be expressed in the following way:

$$P^*=\frac{\rho}{\beta}-\frac{2\pi\rho^2}{3}\int_0^\infty r^3\phi'(r)g^*(r)dr-C. \tag{8}$$

Here ρ is the number density N/V and g^* is the pair correlation function for the constrained system,

$$\rho^2 g^*(r_{12})=N(N-1)\frac{\int\cdots\int e^{-\beta(\Phi_N+W_N)}d\mathbf{r}_3\cdots d\mathbf{r}_N}{\int\cdots\int e^{-\beta(\Phi_N+W_N)}d\mathbf{r}_1\cdots d\mathbf{r}_N}, \tag{9}$$

and generally g^* will differ from the unconstrained-system pair correlation function g. The constraint also affects the pressure by generating the new term C,

$$C=\frac{\int_0^1 ds_{1x}\cdots\int_0^1 ds_{Nz}e^{-\beta(\Phi_N+W_N)}(\partial/\partial V)W_N(V^{1/3}s_{1x}\cdots V^{1/3}s_{Nz})}{\int_0^1 ds_{1x}\cdots\int_0^1 ds_{Nz}e^{-\beta(\Phi_N+W_N)}}. \tag{10}$$

If $W_N(\mathbf{r}_1\cdots\mathbf{r}_N)$ depends on the relative positions of the N particles, but has no explicit dependence on volume V, then the integrand in the numerator of expression (10) for C will vanish everywhere except at the discontinuity hypersurface of W_N. Consequently, the numerator integral reduces to an integral over that $(3N-1)$-dimensional hypersurface of the N-particle probability function weighted by an amount determined by the specific form of W_N. When this type of constraint is applied to the metastable-state problem, the discontinuity hypersurface should occur where the N-particle probability is small, at least for the modest extent of metastability, as argued above. Then the contribution C to the pressure should likewise be small.

An alternative class of constraint functions W_N has volume appearing explicitly as a scaling factor. Specifically,

$$W_N\equiv F(V^{-1/3}\mathbf{r}_1\cdots V^{-1/3}\mathbf{r}_N), \tag{11}$$

and in this event the key factor in the numerator integrand of Eq. (10) is

$$\frac{\partial}{\partial V}F(\mathbf{s}_1\cdots\mathbf{s}_N)\equiv 0. \tag{12}$$

Consequently, C vanishes identically for this class of constraints and it is only the difference between g^* and g that reflects the presence of the constraint. In the following sections we consider special choices for each of these two classes of constraints.

III. EQUATION OF STATE IN THE INHERENT-STRUCTURE VOID-CONSTRAINED ENSEMBLE

A. Inherent structures

The determination of the equilibrium properties of a superheated liquid requires that void formation be suppressed. Therefore, the constraint W_N should be chosen such that bubbles of some critical size (i.e., large enough to allow for the spontaneous formation of the vapor phase) are discouraged from developing, a method quite analogous to the experimental techniques used to study superheated liquids. Yet, the rigorous evaluation of the constrained partition function [Eq. (3)] using the above definition of W_N is, in general, impossible for nontrivial systems. Fortunately, while most constraints are difficult to apply analytically, they are easily imposed in computer simulations.

Previous computer simulation studies [14,17] have analyzed the effect of one such constraint, the void-constrained ensemble, on the equation of state of the superheated Lennard-Jones liquid. In this ensemble, limits are placed on the maximum size of voids that are allowed to form in the liquid. If the largest such void was less than 1.5 times the average interparticle separation, it was found that the system was overconstrained and artificially high tensions resulted (i.e., the pressure was a function of the severity of the constraint); if larger voids were allowed to develop, then the equation of state was found to be essentially independent of the constraint. Overconstrained systems were found to be easily identified by analyzing the distribution of void sizes within the superheated liquid. As long as the void distribution had a well-developed, large void tail (i.e., sampling of configurations that contain voids in excess of an average interparticle separation), the pressure was independent of the constraint. In contrast, artificially high tensions were produced when the constraint yielded abruptly interrupted void distributions, in which the second inflection point in the void size distribution, associated with the appearance of the large void tail was absent.

Clearly, the use of the void-constrained ensemble is not the only means by which one can eliminate bottelnecks to the vapor phase in a superheated liquid. Recently, it has been suggested that a constrained form of the inherent structure formalism can be used to obtain the equilibrium properties of superheated liquids [15]. Stillinger and Weber [10] discussed the separation of the dynamics of liquids into two distinct contributions: sampling of various local minima of the potential energy hypersurface and thermal vibrations about these minima. The mechanically stable configurations of particles at the local minima are called inherent structures and correspond to those states in which the net force on each particle is zero. In fact, the potential energy hypersurface can be divided into ''basins,'' which surround each inherent structure. At a given instant, the configuration of particles can be uniquely assigned to a given basin by following a steepest-descent trajectory and, hence, mapping the configuration to the corresponding local potential energy minimum. As the system evolves, the system configuration will sample various basins along the potential energy hypersurface. While in the basin, if the system is not found at the local minimum, the displacement from the minimum is simply regarded as a ''vibrational'' displacement, most likely anharmonic in character. In other words, at any given instant the system is vibrating about a local potential energy minimum. Therefore, the properties of the liquid are completely determined in principle by the sampling of successive local energy minima plus contributions due to the anharmonic vibrations about these minima.

In Ref. [15] constraints were applied to the inherent structures in order to study metastability. Considering the one-dimensional Lennard-Jones fluid, it was noticed that for densities greater than a certain value ρ_o (where $\rho=N/L$, L being the system length), the system possessed only a single type of potential energy minimum, namely, the regular and periodic arrangement of particles that spanned the system length.

For densities less than ρ_o, however, two types of inherent structures were possible. The periodic arrangement of particles can be maintained below ρ_o, causing the potential energy local minimum to rise in value as the system is stretched. However, another configuration of particles at a local energy minimum can be formed, corresponding to an arrangement of broken chains. The broken chains yield absolute minima, while the unbroken periodic arrays yield higher-lying relative potential-energy minima. The stretched periodic array loses its mechanical stability at a density, $\rho_1 < \rho_o$. Hence, the one-dimensional Lennard-Jones fluid for $\rho_1 \leqslant \rho \leqslant \rho_o$ that has an unbroken periodic inherent structure is equivalent to a stretched metastable state. Therefore, it is reasonable to assume that removing from the partition function configurations that have inherent structures containing large voids, for systems capable of exhibiting a first-order liquid-vapor phase transition, should allow one to rigorously obtain the properties of the metastable liquid [15]. Disallowing the liquid to sample those configurations that map onto inherent structures that contain voids larger than some specified size serves to suppress the vaporization transition and keep the liquid homogeneous within the metastable region. Therefore, following the suggestion outlined in [15], we utilize the inherent structure formalism to obtain the equilibrium properties of a model superheated liquid and analyze the effect of the severity of the constraint, consisting of suppressing the formation of voids in the inherent structure, on its equation of state.

Mathematically, the various local potential energy minima, or inherent structures, are solutions to [10]:

$$\nabla \Phi_N(\mathbf{r}_1 \cdots \mathbf{r}_N) = 0, \tag{13}$$

where $\nabla \Phi_N$ is the gradient of the potential energy Φ_N. Each inherent structure is included in the set of stable packings, within which the force on every particle vanishes. [Note that saddle points and potential-energy maxima are also solutions to Eq. (13).] The number of distinct Φ_N minima is enormous, of the order of $N! e^N$ distinguishable particle packings [18]. $N!$ accounts for particle permutations that yield minima of identical potential energy; e^N estimates the number of distinct ways of arranging particles in mechanically stable packings. Most of these packings are amorphous; others will correspond to defective crystals at slightly lower values of Φ_N. Those inherent structures that are perfect crystals will be the absolute minima in the potential energy.

Each configuration of N particles can be assigned uniquely (mapped) to its own inherent structure. The procedure for finding the proper local minimum is to move the particles along the steepest direction on the Φ_N hypersurface until the forces on each particle vanish. This procedure is equivalent to quenching the system of N particles from an initial temperature T to a final value of $T=0$. As a result, all kinetic energy is removed, leaving the system at rest at a Φ_N minimum. In the case of identical structureless spherical particles, the appropriate mapping is generated by the following steepest-descent equations for each particle i [19]:

$$\frac{d\mathbf{r}_i(s)}{ds} = -\nabla \Phi_N[\mathbf{r}_1(s) \cdots \mathbf{r}_N(s)], \tag{14}$$

where $s \geqslant 0$ is a progress variable indicating the extent to which the descent trajectory has been followed. Starting from an initial configuration ($s=0$), a positive value of s displaces the configuration along the direction of the negative of the potential energy gradient until it comes to rest ($s \to \infty$) at the appropriate minimum. Given an initial configuration of N particles, the simultaneous solution of the N equations in Eq. (14) quenches the system into a potential energy minimum, yielding the appropriate inherent structure.

Steepest-descent trajectories [Eq. (14)] of the shifted-force Lennard-Jones fluid (discussed below) were generated using a conjugate gradient method [20]. The conjugate gradient method is highly efficient during the initial part of the quench, rapidly decreasing the potential energy to within 5% of the true minimum. At this point, however, a large computational effort is required to further decrease the potential energy towards its value at the local minimum. Fortunately, an important simplification results over the range of densities explored in this work, once the potential energy is quenched to within approximately 2% of the true local minimum. Under these conditions, we found that the configuration of particles is essentially identical to the inherent structure. The remainder of the descent trajectory involves only minor adjustments of particle positions so that the force on each particle vanishes exactly. Over the range of densities explored in this work, we found that stopping the quench via the conjugate gradient method when the potential energy was within 1–2 % of the true potential energy minimum yielded quenched configurations that were virtually indistinguishable from the inherent structures. Each iteration of the conjugate gradient method causes a decrease in the potential energy. The quench was terminated when a new iteration yielded a decrease in the potential energy of less than 0.001%. At this point, the energy was within 1–2 % of the true local minimum. Using this approach, the time required to converge to a local minimum for a system composed of 256 particles was as short as 20 min on a HP715 workstation.

The computer simulation studies discussed in this paper were performed using the shifted-force Lennard-Jones 12-6 potential. The Lennard-Jones 12-6 potential is defined by

$$u_{\mathrm{LJ}}(r) = 4\epsilon \left[\left(\frac{\sigma}{r} \right)^{12} - \left(\frac{\sigma}{r} \right)^{6} \right], \tag{15}$$

where r is the distance between two particles, σ the distance at which the potential is zero, and ϵ the well depth. Normally, the Lennard-Jones 12-6 potential is truncated beyond a given cutoff distance r_c. Numerical instabilities, however, are introduced during a descent trajectory using the truncated Lennard-Jones potential, since the force between two particles changes discontinuously at r_c. To avoid this problem, we instead simulated a fluid whose particles interact via the shifted-force Lennard-Jones potential $u_{\mathrm{sf}}(r)$, in which [28]

$$u_{\mathrm{sf}}(r) = \begin{cases} u_{\mathrm{LJ}}(r) - u_{\mathrm{LJ}}(r_c) - (r - r_c) u'_{\mathrm{LJ}}(r_c), & r \leqslant r_c \\ 0, & r > r_c \end{cases} \tag{16}$$

and $u'_{\mathrm{LJ}}(r_c)$ is the value of the derivative of the Lennard-Jones 12-6 potential u_{LJ} at r_c [Eq. (15)]. The shifted-force potential is now such that the potential and force both go

TABLE I. Comparison of the critical and triple-point parameters of the $r_c = 2.5\sigma$ shifted-force Lennard-Jones fluid (SF) and the Lennard-Jones fluid (LJ). The triple-point parameters were obtained using the solid-liquid phase equilibrium data of Kofke [25]. $\rho^*_{\mathrm{tr,\,liq}}$ is the density of the liquid at the triple point. $\rho^* = \rho\sigma^3$, $T^* = kT/\epsilon$, and $P^* = P\sigma^3/\epsilon$. The numbers in parentheses indicate the error in the last one or two digits of the data.

	SF	LJ
ρ^*_c	0.247	0.304(6)
T^*_c	1.16	1.316(4)
P^*_c	0.109	0.130(10)
T^*_{tr}	0.687	0.685(3)
$\rho^*_{\mathrm{tr,\,liq}}$	0.670	0.85(2)

smoothly to zero at the cutoff r_c, eliminating any problems in the convergence towards the appropriate inherent structure. Of course, the properties of the shifted-force Lennard-Jones fluid are different from the Lennard-Jones fluid. For example, since the well depth of the shifted-force potential is shifted slightly upwards to -0.93ϵ (as opposed to $-\epsilon$ for the Lennard-Jones potential) for $r_c = 2.5\sigma$, one expects the value of the critical temperature to be lower than that of the Lennard-Jones fluid. Table I compares the critical and triple-point parameters of the shifted-force fluid with $r_c = 2.5\sigma$ to those of the Lennard-Jones fluid. The equation of state of the shifted-force Lennard-Jones fluid was estimated using a procedure suggested elsewhere [21]: if one assumes that the radial distribution functions of the shifted-force and Lennard-Jones fluid are identical, then the pressure of the shifted-force fluid P_{sf} is equal to [22]

$$P_{\mathrm{sf}} = \rho kT - \frac{2\pi\rho^2}{3}\int_0^{r_c} r^3 \frac{du_{\mathrm{sf}}}{dr}\, g(r)\, dr, \tag{17}$$

where $g(r)$ is the radial distribution function of the Lennard-Jones, calculated by using perturbation theory [23,24]. Vapor-liquid equilibrium properties were obtained by equating pressures and chemical potentials, the latter calculated by integration of Eq. (17). Triple-point parameters were obtained from Eq. (17) and a pressure-temperature expression of the liquid-solid coexistence curve determined from simulation [25].

B. Simulation method

We now compare the results of applying the void constraint on the unquenched and quenched configurations of the superheated shifted-force Lennard-Jones liquid (void-constrained and inherent-structure void-constrained ensembles, respectively). In the former, voids exceeding a given size are prevented from forming within any instantaneous configuration of the liquid. In the latter, the liquid is prevented from sampling those configurations that are mapped to inherent structures containing voids that exceed some specified size. The success of both sets of simulations hinges upon the development of an efficient void-counting algorithm. As described in an earlier study [14], we quantify the size of voids within a given configuration by performing a Voronoi-Delaunay tessellation [26,27]. The Voronoi-Delaunay tessellation is defined as follows: a point $\mathbf{x}$ (where $\mathbf{x}$ is a vector denoting location in space with respect to some origin) belongs to the Voronoi cell of atom i located at position $\mathbf{x}_i$ if it is closer to $\mathbf{x}_i$ than to any other point $\mathbf{x}_j$ of the system. Mathematically, this can be represented by [27]

$$\mathbf{x} \in V_i \Leftrightarrow |\mathbf{x}-\mathbf{x}_i| \leq |\mathbf{x}-\mathbf{x}_j|, \quad \forall j, \tag{18}$$

where V_i denotes the Voronoi polyhedron which surrounds atom i. The dual Delaunay construction is a tiling of space by simplices (d-dimensional tetrahedra where d is the system's dimension), whose vertices are the atom positions $\mathbf{x}_i$, while the centers of the spheres circumscribing these simplices are the Voronoi vertices. The diameter of the circumsphere minus the Lennard-Jones diameter σ is taken as the effective size of a void about a Lennard-Jones particle. For convenience, these voids were visualized as spherical particles with diameters equal to their effective lengths. Figure 1 illustrates the dual tessellation and the definition of a void size.

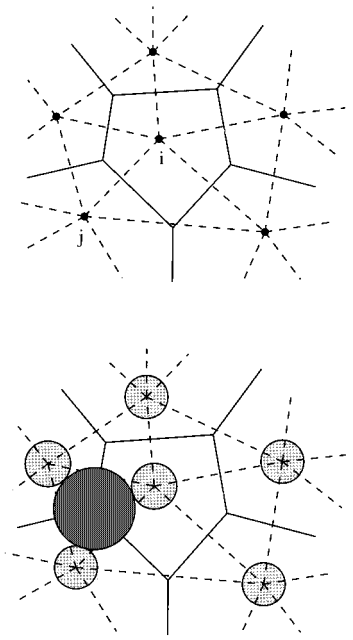

FIG. 1. (top) Two-dimensional illustration of the Voronoi-Delaunay dual construction. The central atom i is surrounded by atoms j. The solid lines form the Voronoi polygon about atom i. The dashed lines form the Delaunay triangles whose circumspheres are centered at the corresponding vertices of the Voronoi polygon. (bottom) The determination of the size (diameter) of ''void particles'' about a Lennard-Jones particle in the superheated liquid. The Lennard-Jones particles lie on the vertices of the Delaunay triangles (smaller shaded circles). The void-particles are centered on the vertices of the Voronoi polygon. For clarity, only one void particle is shown (larger shaded circle). Its diameter equals that of the sphere circumscribing the Delaunay triangle and centered on the vertex of the Voronoi polygon, minus the Lennard-Jones diameter σ. (Figure taken from [14].)

In both constrained ensembles, the relevant parameter is the diameter of the maximum allowed void, $d^*_{\mathrm{max}} = d_{\mathrm{max}}/\sigma$. It is convenient to reference d^*_{max} to the average interparticle separation $(\rho^*)^{-1/3} = (\rho\sigma^3)^{-1/3}$ to obtain the dimensionless variable $b = d_{\mathrm{max}}\rho^{1/3}$. The parameter b simply quantifies the

severity of the constraint; the smaller the value of b, the more severely constrained is the superheated liquid. An additional advantage is gained by expressing the constraint in terms of b rather than $d^*_{\max}$. Since b scales with $(\rho^*)^{-1/3}$, or equivalently $V^{1/3}$, the nonstructural contribution to the pressure arising from the application of the constraint [that is to say, the quantity C in Eq. (10)] is identically zero. The void constraint applied to inherent structures, however, is not strictly of the form shown in Eq. (10), since its position variables are not those of the canonical distribution that is used to derive the equation of state, but rather a function of the mapped position variables. Consequently, one cannot rigorously appeal to Eq. (10) to argue that the term C vanishes identically. Yet, it is not unreasonable to assume, as a first approximation, that the mean linear dimension of the steepest-descent basins scales as $V^{1/3}$; therefore the inherent-structure void constraint (which eliminates entire basins) should involve a negligibly small term C in the equation of state [Eq. (8)]. In what follows, we calculate inherent-structure void constraint pressures using Eq. (8) with $C=0$; the effect of the constraint should only be felt through the virial, since this term is a function of the radial distribution function of the constrained liquid.

Simulations of the superheated shifted-force Lennard-Jones liquid in both the void-constrained and inherent-structure void-constrained ensembles were performed using the canonical Monte Carlo algorithm [28] (constant N, V, and T). The equation of state was determined in both ensembles for a system size of $N=256$ and for two subcritical temperatures: $T^*=0.70$ and $T^*=0.90$. In the void-constrained ensemble, normal Monte Carlo procedures were followed except that a particle move was rejected if that move created a void larger than some specified size. Ensemble averages were calculated over 4000 Monte Carlo steps per particle (MCS) after an initial equilibration period of 1000 MCS.

In the inherent-structure void-constrained ensemble, preventing the sampling of liquid configurations having inherent structures containing large voids requires that the liquid be frequently quenched to the local potential energy minima. In principle, that would require that, after each particle move, the inherent structure of the new liquid configuration and its maximum void size be determined. Such a large number of quenches, even for a system size of $N=256$, is computationally prohibitive. Fortunately, there is no need to perform quenches so frequently. The dynamics of transitions between substantially different inherent structures is relatively slow. During a molecular-dynamics simulation of a 32-particle system, Stillinger and Weber [18] found that the number of transitions between distinct potential energy minima was approximately 250 out of a total run of 10^4 time steps at a temperature 50% greater than the melting temperature. Though they simulated systems at high densities (at or near the liquid-solid transition), it is not unreasonable to assume that the dynamics of transitions between inherent structures of superheated liquids, at densities lower than the triple-point density of the liquid and at subcritical temperatures, is also sluggish. Therefore, during a Monte Carlo simulation, quenches were performed every 100 MCS. To check the validity of the proposed simulation results, we calculated the pressure for simulations in which quenches were performed every 50 MCS. The results were statistically indistinguishable. Simulations at a higher frequency of quenches than 50 MCS were not performed, since, as we will discuss in the following subsection, pressures obtained while quenching every 100 MCS within the inherent-structure void-constrained ensemble were consistent with pressures obtained in the void-constrained ensemble for appropriate choices of the severity of the constraint.

Simulations within the inherent-structure void-constrained ensemble are performed with a Monte Carlo simulation algorithm. The simulation begins with an initial configuration that is mapped to an inherent structure that has no voids exceeding some specified size. For 100 MCS, configurations of the liquid are sampled according to normal Metropolis guidelines. At the end of the 100-MCS block, the liquid is quenched to its inherent structure. A Voronoi-Delaunay tessellation indicates the largest void size within the inherent structure. If the maximum void is less than the specified value, then the properties of the liquid (e.g., pressure and configurational energy) accumulated over the 100-MCS block are counted towards the simulation's ensemble averages. If the void exceeds the given size, then the accumulated averages are discarded. The simulation proceeds with another 100 MCS but starts with the initial configuration of particles used at the beginning of the previous 100-MCS block. Each simulation began with 1000 MCS of equilibration followed by 3000 MCS of ensemble averaging. Thus, 30 quenches were performed in determining the equilibrium properties of the constrained superheated liquid. During equilibration, the total number of MCS was increased if more than half of the quenches yielded rejections. Therefore, we were assured that at least 500 MCS were used to reach equilibration. After equilibration, we found that, for loosely constrained systems (the diameter of voids allowed to form in inherent structures was equal to five or six interparticle distances), on the order of 0–2 quenches resulted in a violation of the constraint (only a small fraction of 100-MCS blocks were rejected). When the liquid was severely constrained (the diameter of voids was less than or equal to four interparticle distances), at most ten quenches resulted in a violation of the constraint (i.e., twenty 100-MCS blocks were counted towards the system's ensemble averages).

Since both constrained ensembles are concerned with the prevention of voids of appreciable size, it is useful to analyze the distribution of void sizes in both the unquenched and quenched liquids. Figure 2 displays the void-size distribution of the unquenched and quenched superheated shifted-force Lennard-Jones liquid at $\rho^*=0.70$ and $T^*=0.70$. Although our approximate equation of state [Eq. (17)] predicts that the density of the liquid at the triple point is $\rho^*=0.670$ ($T^*_{\rm cr}=0.687$), we obtained a slightly negative pressure for simulations at $T^*=0.7$ and $\rho^*=0.725$. From simulation data, we estimate that the density of the liquid at the triple point ($T^*=0.687$) is closer to $\rho^*=0.730$. Voids forming within the liquid (unquenched) rarely exceed two particle diameters; furthermore, the distribution is unimodal and almost symmetrical about the most probable void diameter (approximately 0.7σ). In contrast, the void-size distribution of the corresponding inherent structure exhibits three distinct features: two sharp peaks at small void sizes ($<1.0\sigma$), a broad shoulder spanning intermediate void sizes (ca. 1.0σ–2.5σ),

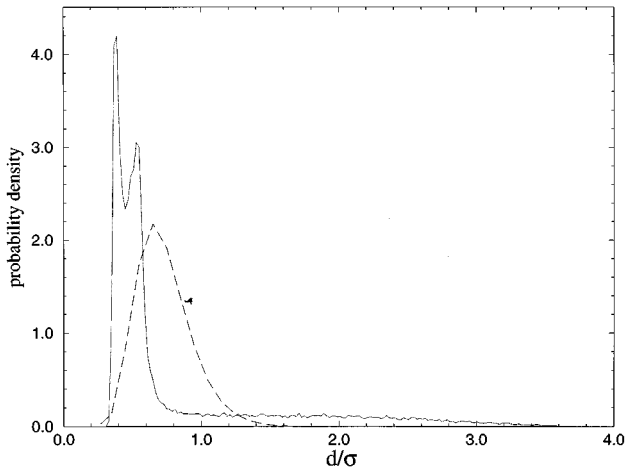

FIG. 2. Probability density of the diameter of voids found in the inherent structure and unquenched liquid of the shifted-force Lennard-Jones fluid at $T^*=0.7$ and $\rho^*=0.7$. The dashed line is the density distribution function of the unquenched liquid.

and a slowly decaying large-void-size tail ($>2.5\sigma$). The inherent structures of a superheated liquid contain voids whose sizes exceed that of the largest voids seen within the unquenched liquid. Therefore, the sizes of voids that must be prevented from forming within inherent structures of the superheated liquid will greatly exceed the sizes of voids prohibited from developing within the unquenched liquid.

TABLE II. Pressure and configurational energy per particle of the shifted-force Lennard-Jones liquid within the inherent-structure void-constrained ensemble for various values of b at $T^*=0.7$. From Eq. (17), the density of the liquid at coexistence is $\rho^*=0.663$; the density of the liquid at the spinodal is approximately $\rho^*=0.506$. The numbers in parentheses indicate the error in the last two or three decimal places.

ρ^*	b	P^*	U^*/N
0.55	4.0	−0.5429(478)	−3.528(167)
0.55	5.0	−0.2376(424)	−3.117(52)
0.55	6.0	−0.2772(504)	−3.194(49)
0.60	4.0[a]	−1.897(888)	−1.956(241)
0.60	5.0	−0.2370(444)	−3.407(68)
0.60	6.0	−0.2451(429)	−3.387(48)
0.65	4.0	−0.3966(638)	−3.602(58)
0.65	5.0	−0.2723(489)	−3.575(37)
0.65	6.0	−0.2711(467)	−3.577(39)
0.70	4.0	−0.3792(463)	−3.859(39)
0.70	5.0	−0.1385(223)	−3.848(40)
0.70	6.0	−0.1880(497)	−3.843(38)
0.725	4.0	−0.06983(472)	−3.977(39)
0.725	5.0	−0.01233(465)	−3.982(37)
0.725	6.0	−0.01619(471)	−3.969(31)

[a]Less than ten 100-MCS blocks used to calculate ensemble averages, due to frequent violation of the constraint.

TABLE III. Pressure and configurational energy per particle of the shifted-force Lennard-Jones liquid within the inherent-structure void-constrained ensemble for various values of b at $T^*=0.9$. From Eq. (17), the density of the liquid at coexistence is $\rho^*=0.545$; the density of the liquid at the spinodal is $\rho^*=0.427$. The numbers in parentheses indicate the error in the last two or three decimal places.

ρ^*	b	P^*	U^*/N
0.55	4.0	−15.19(39)	−7.968(47)
0.55	5.0	0.06622(5091)	−2.934(44)
0.55	6.0	0.06555(4939)	−2.931(46)
0.60	4.0	−4.825(458)	−4.465(127)
0.60	5.0	0.1483(516)	−3.181(42)
0.60	6.0	0.1505(531)	−3.179(44)
0.65	4.0	0.1114(792)	−3.426(59)
0.65	5.0	0.2951(555)	−3.431(45)
0.65	6.0	0.3038(514)	−3.433(43)
0.70	4.0	0.4349(568)	−3.750(55)
0.70	5.0	0.5530(514)	−3.688(44)
0.70	6.0	0.5547(548)	−3.694(58)
0.725	4.0	0.7121(542)	−3.831(47)
0.725	5.0	0.7498(544)	−3.820(46)
0.725	6.0	0.7403(567)	−3.821(54)

C. Results

Simulations at two subcritical temperatures ($T^*=0.7$ and 0.9) were performed at various densities for $b=1.0$, 1.5, 2.0 within the void-constrained ensemble and for $b=4.0$, 5.0, 6.0 within the inherent-structure void-constrained ensemble. Values of the pressure P^* and configurational energy per particle U^*/N were determined at each density and severity of the constraint b. Simulations at $T^*=0.9$ were performed for densities well within the metastable region and for densities just below that of the liquid at the triple point. Simulations at $T^*=0.7$ were performed within the metastable region and for some densities inside the unstable region.

At each temperature studied, the pressure within the inherent-structure void-constrained ensemble is extremely sensitive to the severity of the constraint b (see Tables II and III). For most densities simulated, pressures obtained for $b=5.0$ and $b=6.0$ are statistically indistinguishable. However, when $b=4.0$ the pressure is drastically reduced, the change being dependent upon the proximity to the superheated liquid spinodal. For example, at $T^*=0.9$ and $\rho^*=0.55$, a state point within the predicted metastable region, the artificially high tension produced for $b=4.0$ is almost two orders of magnitude larger than the pressures obtained for $b=5.0$ and $b=6.0$. Similar trends, though not as pronounced, are seen for the configurational energy per particle. This extreme sensitivity of the thermophysical properties of the stable and metastable liquid is quite remarkable, given the fact that we are preventing infrequently visited configurations with large voids in the inherent structures. Thus, we see that large voids in inherent structures are extremely important in determining the correct equilibrium properties of the liquid state.

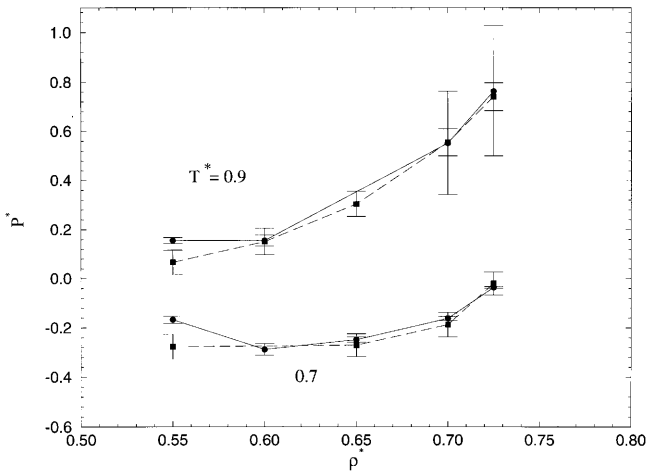

FIG. 3. Comparison of the equation of state of shifted-force Lennard-Jones fluid in both the void-constrained and inherent-structure void-constrained ensembles. The solid lines (filled circles) are the equation of state within the void-constrained ensemble for $b=2.0$. The dashed lines (filled squares) are the equation of state within the inherent-structure void-constrained ensemble for $b=6.0$.

As found for the Lennard-Jones liquid in a previous study [14], the equation of state of the superheated shifted-force Lennard-Jones fluid within the void-constrained ensemble was insensitive to values of $b>1.5$, but yielded artificial tensions when $b<1.5$. Figure 3 compares the equation of state of the shifted-force liquid for $b=2.0$ (prevention of voids in the instantaneous configurations) with the equation of state for $b=6.0$ (prevention of voids in the corresponding inherent structures). We see that the two sets of simulations, within error bars, yield similar results. Though pressures for $b=5.0$ are not shown in Figure 3, we conclude, since $b=5.0$ and $b=6.0$ produce statistically indistinguishable results (see Tables II and III), that in order to obtain the true equation of state of the superheated liquid, voids of at least five interparticle separations ($b>5.0$) must be allowed to form in the inherent structure. In addition, we obtain consistency between two different kinds of constraints: prevention of voids within the liquid and within the corresponding inherent structures serve to suppress cavitation and allow the superheated liquid to reach equilibrium.

In [14], the distribution of voids within the instantaneous, unquenched superheated liquid provided a way in which one could objectively determine whether a system was overconstrained (i.e., yielded artificially high tensions). As long as the void distribution has a well-developed large-void tail (i.e., the liquid is able to sample those configurations that have voids with diameters greater than the average interparticle distance), the pressure is independent of the constraint. Constraints that result in abruptly interrupted void distributions, in which the second inflection point associated with the tail of the distribution is absent, lead to artificially high tensions. The appearance or disappearance of the second inflection point of the void-size distribution provides a clear geometric criterion for determining whether a constraint is unphysical. Unfortunately, there is no correspondingly simple criterion for simulations in the inherent-structure void-constrained ensemble. Simulations for $b=4.0$ produce artificially low pressures, while $b=5.0$ and $b=6.0$ yield statistically indistinguishable results. Yet, simulations with $b=4.0$ do not prevent the formation of a well-developed large-void tail (see Fig. 2). Except for the largest void sizes sampled, the void-size distributions for all choices of b are equivalent. Thus, there does not appear to be a simple geometric criterion for determining *a priori* whether the superheated liquid within the inherent-structure void-constrained ensemble is overconstrained.

IV. STATISTICAL GEOMETRY OF INHERENT STRUCTURES

The distribution of void sizes within inherent structures is quite different from that of the instantaneous, unquenched liquid (see Fig. 2). Inherent structures contain large voids that never form within the unquenched liquid. The narrow double-peaked profile at small void sizes, along with the broad shoulder spanning moderate void diameters, is clearly not seen in the unquenched system. Yet, the sampling of local potential energy minima containing large voids (in excess of five average interparticle separations) is important in determining the equilibrium properties of both stable and superheated liquids. We are therefore interested in studying the statistical geometry of voids within inherent structures of both stable and metastable liquids. Consequently, we address several questions: Is the void-size distribution a function of the temperature (particularly as one moves, at constant density, from a point within the metastable region to one lying in the stable region of the phase diagram), in addition to density? Do the large voids disappear as the range of the intermolecular potential is increased? Are the large voids within inherent structures isolated, or are they connected? In investigating these questions, we analyze the importance of local potential energy minima in determining the equilibrium properties of both stable and metastable liquids for densities up to the density of the liquid at the triple point.

Inherent structures (which are equivalent to infinitely rapid quenches of the system to $T=0$) in Lennard-Jones-like systems have been found to be substantially invariant with respect to the starting temperature [10]. To confirm this, we calculated the distribution of void sizes for several state points along an isochore, increasing the temperature from an initial point within the metastable region towards a final point well above the critical temperature of the liquid. Figure 4 shows the void-size distribution of inherent structures at $\rho^*=0.725$ (a density just below that of the liquid at the triple point) for several values of the temperature, ranging from just above the triple-point temperature to approximately twice the critical temperature. We clearly see that the distribution of void sizes is independent of temperature. Nevertheless, what is remarkable about Fig. 4 is that for $T^*=0.7$ the system is metastable and at $T^*=0.9$ and 1.84 the system is in the one-phase region. Therefore, we find that a stable liquid, slightly below its triple-point density, has inherent structures that contain extremely large voids. The appearance of large cavities in the inherent structure of a highly metastable liquid (high tension) might be expected, since a stretched liquid relieves tension by forming cavities (i.e., the metastable liquid phase-separates via cavitation). Yet, it is sur-

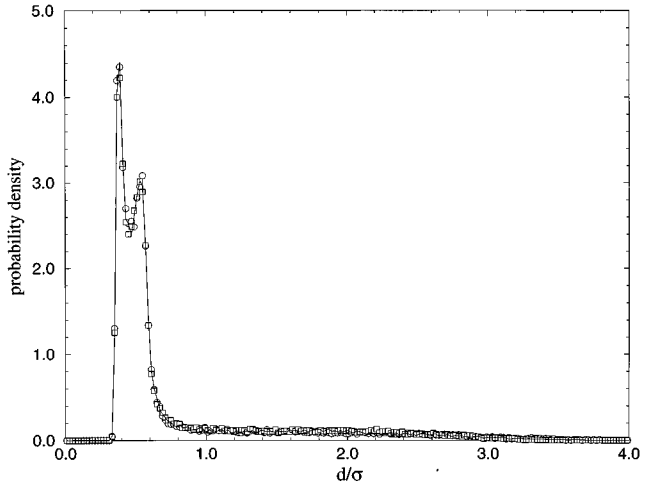

FIG. 4. Void-size distribution of the inherent structures of the shifted-force Lennard-Jones liquid for three temperatures at a density of $\rho^*=0.725$. The solid line is the distribution at $T^*=0.7$; the open circles are for $T^*=0.9$; the open squares are for $T^*=1.84$.

prising to find that a thermodynamically stable liquid, when quenched, contains the same large cavities as a metastable system. In other words, a stable liquid samples potential-energy basins that contain voids in excess of several molecular diameters.

The void-size distributions of inherent structures in Fig. 4 provide no information on the spatial distribution of cavities. Hence, we are interested in understanding how the large voids are arranged: are they isolated or connected, possibly spanning the length of the simulation cell? Figure 5 shows a

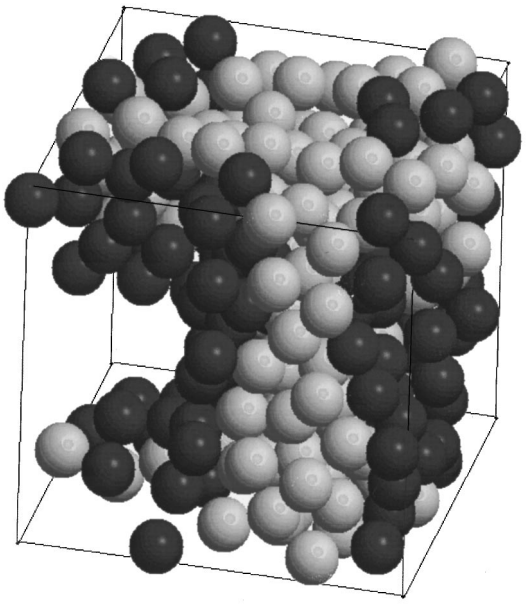

FIG. 5. Snapshot of a configuration of $N=256$ particles interacting via the shifted-force Lennard-Jones intermolecular potential quenched to the potential energy minimum for $T^*=0.9$ and $\rho^*=0.725$. For clarity, particles adjadcent to a void exceeding 1.0σ are shaded darker; the remaining particles are lighter. The solid lines indicate the edges of the simulation cell.

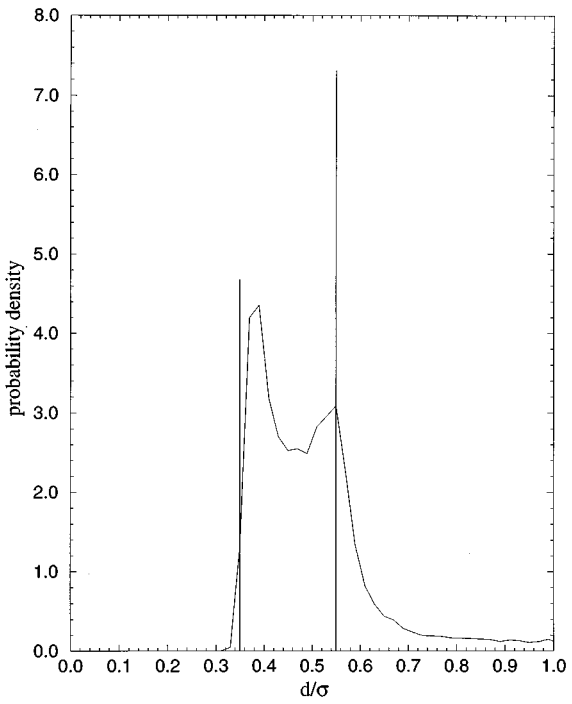

FIG. 6. Void-size distribution of the inherent structure at $\rho^*=0.725$ and of the face-centered-cubic crystal at $\rho^*=1.0577$ for the shifted-force Lennard-Jones potential. The two spikes at $d/\sigma=0.35$ and $d/\sigma=0.55$ constitute the void-size distribution of the face-centered-cubic crystal. They are scaled by a factor of 4.

configuration of particles quenched to a potential-energy minimum for $N=256$ and $\rho^*=0.725$. In the figure, particles that are adjacent to a void exceeding 1.0σ in diameter are colored dark grey. We clearly see that for $N=256$, taking into account the periodic boundary conditions, there is a single nonconvex cavity that spans the entire simulation cell. The dark particles form an interface, dividing the system into a compact region (dark and light particles) and a void region (empty space). Due to the appearance of the void, the compact region has a higher density than the original system and is solely responsible for the narrow double peak found in the void-size distributions (Fig. 4).

The compact region is a dense amorphous arrangement of particles exhibiting a narrow bimodal distribution of void sizes. The origin of this double-peaked structure can be found in the distribution of voids of the face-centered-cubic (fcc) crystal, since the shifted-force Lennard-Jones liquid crystallizes into an fcc arrangement [25]. In other words, the inherent structure located at the global minimum of the potential-energy hypersurface is a fcc crystal. Figure 6 compares the void-size distribution of the fcc crystal at a density of $\rho^*=1.0577$ with the void-size distribution of an inherent structure at $\rho^*=0.725$. The shifted-force Lennard-Jones fcc crystal exhibits its lowest potential energy per particle at $\rho^*=1.0577$. The void-size distribution of the fcc crystal exhibits only two spikes at void sizes of $d/\sigma=0.35$ and 0.55. These spikes correspond to the presence of tetrahedral and octahedral voids, respectively [29], in the fcc crystal. A tetrahedral void is formed when four particles are arranged at the corners of a tetrahedron. An octahedral void is sur-

rounded by six spheres, located at the corners of an octahedron. Though the first and second peaks of the distribution of the liquid's inherent structure are not aligned exactly with the fcc crystal's void-size distribution (indicating some packing disorder, and that the density of the compact region is different from the chosen density of the fcc crystal), it is clear that the inherent structure's bimodal distribution is related to the voids in the fcc crystal. In fact, the double-peaked distribution is caused by the formation of distorted tetrahedra and octahedra. Using the algorithm of Sastry *et al.* [30] to calculate the volume of the void regions in the inherent structures for a bulk density of $\rho^* = 0.725$, we find that the density of the compact region of inherent structures is $\rho^* = 0.838 \pm 0.034$. Although it is still less dense than the crystal at the global minimum, the compact region exhibits particle arrangements similar to those found in the fcc crystal. Of course, the tetrahedra and octahedra comprising the compact region show continuously varying degrees of distortion. This is an expected result of dense amorphous packing, where short-range order is present but long-range order is absent.

It is interesting to note that the characteristic double peak found in the void-size distributions of inherent structures was also seen by Finney and Wallace [31] in a study of dense random packings of soft spheres. Finney and Wallace analyzed the size of voids within a dense arrangement of hard spheres near random close packing. The distribution of void sizes for this system was unimodal. However, as this arrangement was allowed to relax under a soft potential, a distinct bimodality developed at small void sizes. Their double-peaked structure is very similar to ours, in which the first peak is larger than the second, indicating that the compact region is forming an amorphous structure.

We have seen that a single large void, spanning the simulation cell, is found for $N = 256$. It is not known whether system-spanning voids persist for larger N values. To address this question, we performed two separate quenches of a system composed of $N = 1372$ particles, equilibrated at $T^* = 0.9$ and $\rho^* = 0.725$. The resulting void-size distribution is shown in Fig. 7. Also included, for comparison, is the distribution for $N = 256$ at the same density. The void-size distributions both display the same characteristic form: a narrow double peak at small void sizes, a broad shoulder at intermediate void diameters, and a slowly decaying large-void tail. In fact, the void-size distribution is approximately system-size independent; minor deviations between the two distributions are found only at small void sizes. The inherent structure of a single quench for $N = 1372$ is shown in Fig. 8. As before, particles adjacent to a void greater than 1.0σ are shaded dark grey and the remaining particles are light grey. We again see, accounting for periodic boundary conditions, that the cavities are indeed connected, forming a single channel that percolates throughout the entire simulation cell. By definition, the dark particles again separate the inherent structure into two distinct regions: a compact region (light and dark) and a void, separated by an interface (dark). The compact and interfacial regions are solely responsible for the double peak of the void-size distribution. The dark particles completely enclose the void region, which gives rise to the broad shoulder and slowly decaying large-void tail.

Figures 5 and 8 have interesting implications. The presence of large voids in the inherent structure means that, from a strictly energetic viewpoint, a thermodynamically stable liquid, even at its triple point, is unstable with respect to the appearance of large voids (''boiling''). Thermal motion prevents the stable fluid from phase-separating. Nevertheless, at low enough temperatures, inherent structures should begin to dominate the properties of the liquid, becoming ultimately responsible for the mechanical weakness of liquids. The pos-

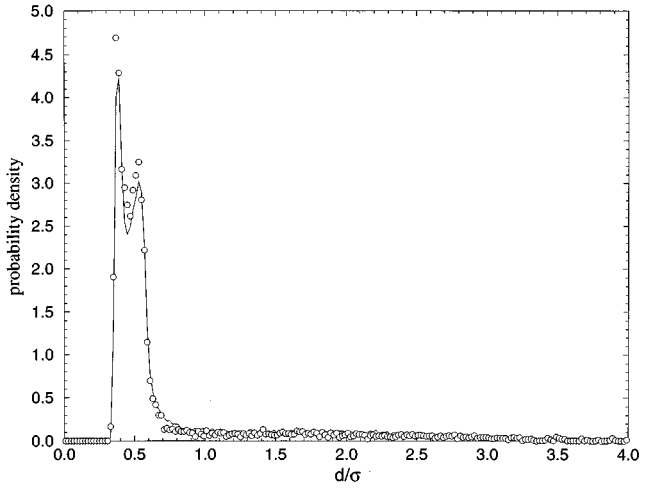

FIG. 7. Void-size distribution of the inherent structure of the shifted-force Lennard-Jones fluid for both $N = 256$ and $N = 1372$ at $\rho^* = 0.725$. Solid line is the distribution for $N = 256$; open circles describe the distribution, obtained from two separate quenches, for $N = 1372$.

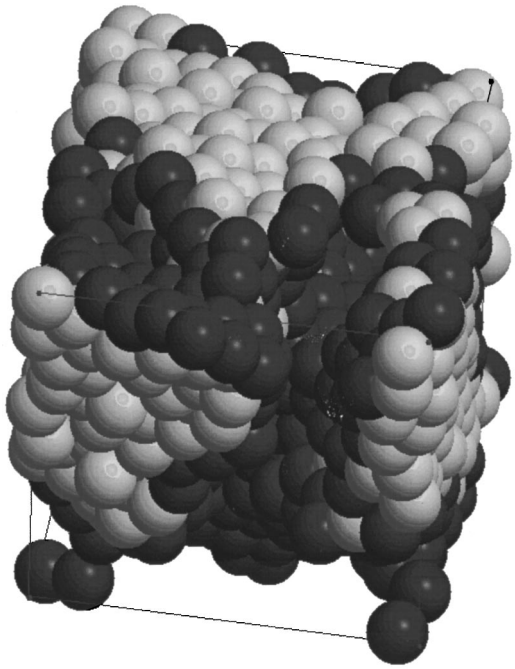

FIG. 8. Snapshot of a configuration of $N = 1372$ particles interacting via the shifted-force Lennard-Jones intermolecular potential quenched to the potential energy minimum for $T^* = 0.9$ and $\rho^* = 0.725$. For clarity, particles adjacent to a void exceeding 1.0σ are shaded darker; the remaining particles are lighter. The solid lines indicate the edges of the simulation cell.

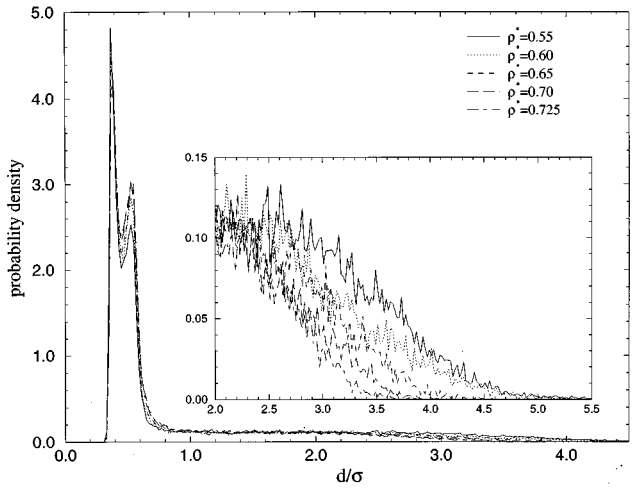

FIG. 9. Inherent-structure void-size distribution of the shifted-force Lennard-Jones liquid for various values of the density.

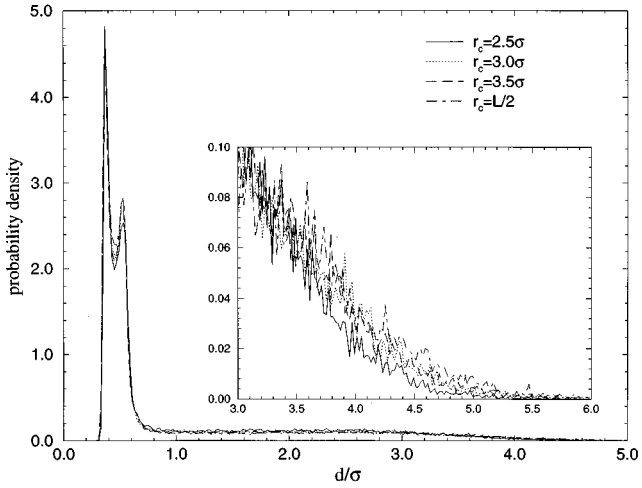

FIG. 10. Inherent-structure void-size distribution of the shifted-force Lennard-Jones potential at $\rho^* = 0.55$ for various values of the cutoff r_c. L is the length of the simulation box.

sibility that ''weak spots'' (small voids) in the instantaneous unquenched liquid are related to the large cavities seen in inherent structures may, if confirmed, shed light on the role of the potential energy hypersurface in determining the tensile strength of liquids at low enough temperatures.

Figure 4 shows that inherent structures are independent of temperature. We now investigate the effect of density on the void-size distribution of inherent structures. Figure 9 displays void-size distributions for various densities, ranging from approximately twice the critical density to just below the triple-point density. The distribution of voids is sensitive to the system density. The large-void tail decays more slowly as the density is decreased (i.e., larger voids appear at lower densities). The distribution of voids within the compact region is also affected by the density. The location and height of the first peak remains invariant to changes in density, but the second peak clearly decreases with a decrease in density. Since the first peak's location does not change, the decrease in the height of the second peak upon decreasing the bulk density indicates a corresponding decrease in the number of octahedral voids in the compact region. In contrast, the number of tetrahedral voids is independent of density. The fewer appearances of octahedral voids, along with a decrease in the decay rate of the large-void tail, suggests that the density of the compact region is increasing as the system density is decreased.

The above discussion pertains to a system with a potential range of $r_c = 2.5\sigma$. In principle, the range of the intermolecular potential r_c should affect the void-size distribution. To investigate this effect, we performed several simulations in which the value of r_c was increased from 2.5σ to one-half the simulation box length. During each simulation several quenches were performed. Figure 10 displays the resulting distribution of void sizes in the inherent structures. As with changes in density, the height of the first peak is independent of the range of the potential but the second peak increases with r_c. In addition, the large-void tail decays more slowly as r_c is increased; a longer-ranged intermolecular potential allows for the formation of larger cavities. The effect of the range of the intermolecular potential on the structure of local potential energy minima may offer insight into the effect of attractive forces on the properties of liquids and amorphous materials. The attractive potential is responsible for the tensile strength of liquids, providing the cohesion necessary to resist stretching (negative pressures cannot be attained in a fluid whose constituent molecules interact via a purely repulsive potential). At the same time, however, the attractive part of the potential is solely responsible for the appearance of large cavities in inherent structures, possibly an important factor in the low-temperature fracture of materials. To gain further insight into this interesting concept, it is important to study the effect of the well depth and the curvature of the intermolecular potential on the void-size distribution in both the instantaneous and quenched configurations of model liquids.

V. CONCLUSIONS

The inherent structure formalism is a useful way of describing molecular dynamics in liquids. The properties of the liquid phase are determined by the sampling of various local potential energy minima (mechanically stable particle packings) and anharmonic thermal vibrations about these minima. Inherent structures also provide a means by which unwanted configurations can be removed from the partition function (imposition of a constraint). Here, we have studied one such constraint: the inherent-structure void-constrained ensemble. In this constrained ensemble, limits are placed on the maximum size of voids allowed to form in the inherent structures of the superheated liquid. The equation of state of the stable and superheated shifted-force Lennard-Jones liquid is extremely sensitive to the severity of the constraint. However, as long as the corresponding inherent structures contain voids in excess of five average interparticle separations, the resulting equation of state is consistent with simulation results in the void-constrained ensemble, in which voids greater than 1.5 times the average interparticle separation are not allowed to form within the instantaneous unquenched liquid. Therefore, the sampling of potential energy basins

that have inherent structures containing voids greater than 5 average interparticle separations is important in determining the equilibrium properties of liquids near the triple point.

The distribution of voids within inherent structures was analyzed to determine whether there is an objective criterion to determine when the system is overconstrained. For the void-constrained ensemble, where voids are prevented from forming within the unquenched liquid, the pressure is independent of the constraint if the void distribution has a well-developed large-void tail. The void-size distribution must include a second inflection point, sampling the infrequently visited yet important large cavities, in order for the liquid to be ''naturally'' constrained. Within the inherent-structure void-constrained ensemble, there is no corresponding geometric criterion to determine if the liquid is overconstrained. For all severities of constraint studied, the slowly decaying large-void tail is always present; the second inflection point, a prerequisite for the development of the large-void tail, occurs at void sizes well below that of the maximum-allowed void diameter (even for the most severely constrained system).

Even at the triple-point density, the presence of large voids (in excess of five average interparticle separations) within the liquid's inherent structures is necessary for the properties of the liquid to attain their true equilibrium values. We therefore analyzed the statistical geometry of voids in inherent structures for stable and superheated liquids at densities between the critical and triple points. The distribution of voids within inherent structures of both the stable and metastable liquids are identical; a thermodynamically stable liquid, even at its triple-point density, samples local potential-energy minima that contain very large cavities. We found that these large cavities are connected, spanning the length of the simulation cell. Hence, strictly from an energetic viewpoint, even a thermodynamically stable liquid is unstable with respect to boiling. This result has potential significance in the study of the fracture of liquids and amorphous solids at low temperatures. In order to investigate this connection, a useful starting point is to study the temperature and tension-dependent correspondence between inherent structure cavities and voids in the unquenched fluid.

The inherent structures of liquids above the triple-point temperature and below their triple-point density are separated into two distinct regions: a compact region, containing all the particles at a density higher than the mean system density, and the void region (a single, particle-free cavity, percolating throughout the system). The compact region is responsible for the bimodal distribution of voids at small void sizes, caused by the formation of distorted tetrahedra (first peak) and octahedra (second peak), found undistorted in the fcc crystal. The void region accounts for the broad shoulder in the distribution, at intermediate void sizes, and the slowly decaying large-void tail. The void-size distribution is a function of the system density and the range of the intermolecular potential. The first peak of the distribution is invariant with changes in the density and the range of the potential; the second peak and large-void tail are sensitive to changes in these variables.

The present work offers insight into the dual role of attractive forces in determining the properties of liquids and amorphous materials. Attractive forces are responsible for the cohesive strength of liquids. Yet, paradoxically, attractions are also (and solely) responsible for the existence of large voids in configurations corresponding to potential-energy minima. Clearly, mapping the range of temperature and tensions where attraction is stabilizing or destabilizing is important.

More generally, this study points to the importance of understanding and investigating the intimate relation between metastability and constraints. Simulations are the natural method for studying the effects of constraints microscopically and hence should become a basic tool in the fundamental investigation of metastability. We believe that much can be learned about the liquid state of matter under both stable and metastable conditions from this type of investigation.

ACKNOWLEDGMENT

P.G.D. gratefully acknowledges the support of the U.S. Department of Energy, Division of Chemical Sciences, Division of Basic Energy Sciences (Grant No. DE-FG02-87ER13714).

[1] J. Frenkel, *Kinetic Theory of Liquids* (Dover, New York, 1955), Chap. 7.
[2] F. F. Abraham, *Homogeneous Nucleation Theory. The Pretransition Theory of Vapor Condensation* (Academic, New York, 1974).
[3] D. W. Oxtoby, Adv. Chem. Phys. **70**, 263 (1988).
[4] P. G. Debenedetti, *Metastable Liquids* (Princeton University Press, Princeton, NJ, 1996).
[5] R. E. Apfel, Sci. Am. **227**, 58 (1972).
[6] *Cavitation and Hydraulic Machinery*, edited by F. Numachi (Institute of High Speed Mechanics, Tohoku University, Sendai, 1963).
[7] *Bubble and Spark Chambers. Principles and Use*, edited by R. P. Shutt (Academic, New York, 1967), Vol. 1.
[8] W. J. Pockman, J. S. Sperry, and J. W. O'Leary, Nature **378**, 715 (1995).
[9] S. J. Putterman, Sci. Am. **272**, 46 (1995).
[10] F. H. Stillinger and T. A. Weber, Phys. Rev. A **25**, 978 (1982).
[11] F. H. Stillinger, in *Mathematical Frontiers in Computational Chemical Physics*, edited by D. G. Truhlas (Springer-Verlag, New York, 1988), pp. 157–173.
[12] T. L. Hill, *Statistical Mechanics* (McGraw-Hill, New York, 1956).
[13] F. H. Stillinger, J. Chem. Phys. **88**, 7818 (1988).
[14] D. S. Corti and P. G. Debenedetti, Ind. Eng. Chem. Res. **34**, 3573 (1995).
[15] F. H. Stillinger, Phys. Rev. E **52**, 4685 (1995).
[16] Ref. [12], pp. 189–191.
[17] D. S. Corti and P. G. Debenedetti, Chem. Eng. Sci. **49**, 2717 (1994).
[18] F. H. Stillinger and T. A. Weber, Phys. Rev. A **28**, 2408 (1983).

[19] F. H. Stillinger and T. A. Weber, J. Chem. Phys. **83**, 4767 (1985).
[20] W. H. Press, S. A. Teukosky, W. T. Vetterling, and B. P. Flannery, *Numerical Recipes*, 2nd ed. (Cambridge University Press, Cambridge, 1992).
[21] J. J. Nicolas, K. E. Gubbins, W. B. Streett, and D. J. Tildesley, Mol. Phys. **37**, 1429 (1979).
[22] D. A. McQuarrie, *Statistical Mechanics* (Harper & Row, New York, 1976).
[23] W. R. Smith and D. Henderson, Mol. Phys. **19**, 411 (1970).
[24] J. D. Weeks, D. Chandler, and H. C. Andersen, J. Chem. Phys. **54**, 5237 (1972); L. Verlet and J. J. Weis, Phys. Rev. A **5**, 939 (1972).
[25] D. A. Kofke (private communications, 1996); J. Chem. Phys **98**, 4149 (1993).
[26] M. Tanemura, T. Ogawa, and N. Ogita, J. Comput. Phys. **51**, 191 (1983).
[27] R. Riedinger, M. Habar, P. Oelhafen, and H. J. Güntherodt, J. Comput. Phys. **74**, 61 (1988).
[28] M. P. Allen and D. J. Tildesley, *Computer Simulation of Liquids* (Clarendon, Oxford, 1992).
[29] K. J. Laidler and J. H. Meiser, *Physical Chemistry* (Benjamin-Cummings, Reading, MA, 1982).
[30] S. Sastry, D. S. Corti, P. G. Debenedetti, and F. H. Stillinger (unpublished).
[31] J. L. Finney and J. Wallace, J. Non-Cryst. Solids **43**, 165 (1981).